Neuron, Volume *104*

Supplemental Information

Postural Representations of the Hand in the Primate Sensorimotor Cortex

James M. Goodman, Gregg A. Tabot, Alex S. Lee, Aneesha K. Suresh, Alexander T. Rajan, Nicholas G. Hatsopoulos, and Sliman Bensmaia

SUPPLEMENTAL INFORMATION

Table S1. *Statistics of pseudo-R^2 values for the generalized linear models (GLMs).* Related to Figure 3. Statistics are shown for neurons with pseudo-$R^2 > 0.05$. For each dataset, we report the number of neurons above this criterion (N), the mean pseudo-R^2 across that population (μ), and its standard deviation (σ). The mean pseudo-R^2 in each dataset is compared to that of the reaching dataset using Welch's two-tailed t-test. The *t*-statistic (*t*), estimated degrees of freedom (*dof*), and *p* value (*p*) are reported for each of these comparisons.

Task and Area	N	μ	σ	t	dof	p
Grasp Area 3a	31	0.185	0.110	2.42	55.8	1.87e-02[a]
Grasp Area 2	41	0.130	0.087	0.15	84.6	8.83e-01
Grasp M1	206	0.185	0.133	3.53	94.2	6.43e-04[a]
Reach M1 (Hatsopoulos et al 2007)[b]	46	0.127	0.091			

---

[a] Significant after applying the Holm-Bonferroni correction for multiple comparisons.

[b] These particular GLM statistics are not reported in the original paper; rather, we fit GLMs to these data using the approach described in the Methods.

Table S2. *List of non-stationary joints present in the musculoskeletal model of the arm.* Related to STAR Methods. We reconstructed the time-varying angles of each degree of freedom of each joint listed here, which in turn were used as separate predictors in generalized linear models (GLM). For each joint, the number of degrees of freedom (# DOF) and set of bones defining that joint are reported.

Joint	# DOF	Bones
Elbow[a]	1	• Humerus • Ulna • Radius
Wrist	3	• Radius • Carpus • Ulna
Carpo-metacarpal (CMC) 1	3[b]	• Carpus • Metacarpal (MC) 1
Metacarpo-phalangeal (MCP) 1	2	• MC 1 • Proximal phalanx (PP) 1
Interphalangeal (IP) 1[a]	1	• PP 1 • Distal phalanx (DP) 1
CMC 4	1	• Carpus • MC 4
CMC 5	3[b]	• Carpus • MC 5
MCP X[c]	2	• MC X[c] • PP X[c]
Proximal IP X[c]	1	• PP X[c] • Middle phalanx (MP) X[c]
Distal IP X[a,c]	1	• MP X[c] • Distal phalanx X[c]

---

[a] Not reconstructed for Monkey 1.

[b] Comprised 2, not 3, degrees of freedom in Monkey 1.

[c] The symbol “X” stands in for one of digits 2-5, each of which was included in the model.

Table S3. *List of muscles present in the musculoskeletal model of the arm.* Related to STAR Methods. We reconstructed the time-varying lengths of each head of each muscle, which in turn were used as separate predictors in generalized linear models (GLM). For each muscle, the number of heads is reported. Muscle length reconstructions were not obtained from Monkey 1.

Muscle	# Heads
Triceps brachii	3
Biceps brachii	2
Anconeus	1
Brachialis	1
Brachioradialis	1
Supinator	1
Pronator teres	1
Pronator quadratus	1
Extensor carpi radialis (ECR) longus	1
ECR brevis	1
Extensor carpi ulnaris	1
Flexor carpi radialis	1
Flexor carpi ulnaris	1
Palmaris longus	1
Extensor digitorum communis	4
Extensor indicis proprius	1[a]
Extensor digiti minimi	1[a]
Flexor digitorum superficialis	4
Flexor digitorum profundus	5[b]
Extensor pollicis (EP) longus	1
EP brevis	1
Abductor pollicis longus	1

---

[a] Use of human model leaves one fewer head than seen in the macaque, where these muscles are replaced by extensor digiti 2-3 and extensor digiti 4-5, respectively.

[b] The fifth head that inserts onto the thumb in monkeys is absent in the human model; the flexor pollicis longus (a muscle that is absent in the monkey) is assumed to comprise this fifth head.

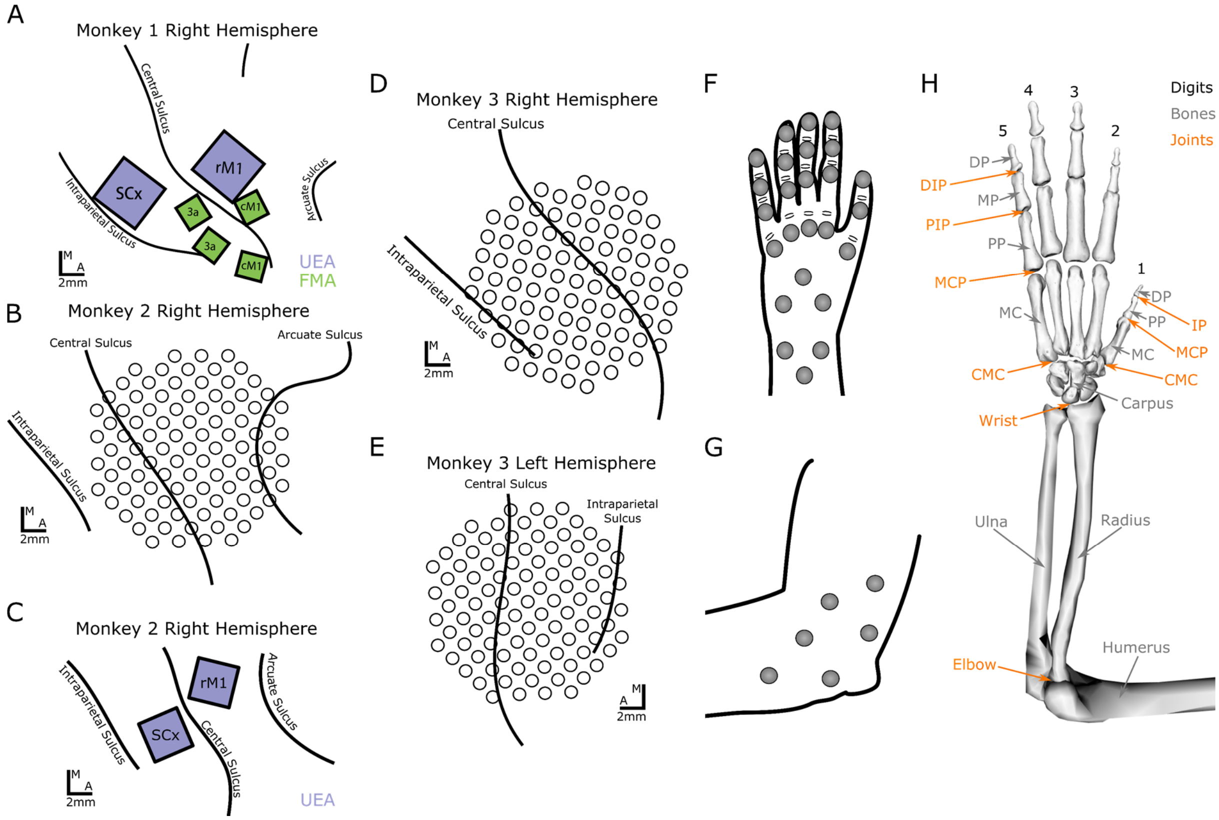

Figure S1. *Array placements and details of kinematic tracking.* Related to Figure 1 and STAR Methods. **(A-E)** Array placements on the cortical surface are shown for **(A)** Monkey 1, **(B)** Monkey 2 (first array), **(C)** Monkey 2 (second array, implanted 3 years after the first), and the **(D)** right and **(E)** left hemispheres of Monkey 3. Figure 1 in the main text displays array placement in Monkey 4, in addition to histological reconstruction of architectonic borders and electrode locations. In scale bar labels, A corresponds to anterior, and M corresponds to medial. **(F-G)** The placements of reflective markers relative to the **(F)** hand and **(G)** elbow. **(H)** A diagram of the skeletal model used for inverse kinematics, with naming conventions matching those in Table S2. Abbreviations of distal joints and bones: DP, distal phalanx; MP, middle phalanx; PP, proximal phalanx; MC, metacarpal; DIP, distal inter-phalangeal joint; PIP, proximal inter-phalangeal joint; IP, inter-phalangeal joint; MCP, metacarpo-phalangeal joint; CMC, carpo-metacarpal joint. Only the joints of the first and fifth digits are explicitly labeled. The bones and joints of digits 2-4 follow the same nomenclature as that of digit 5. Digit 1 is an exception as it comprises just two phalanges.

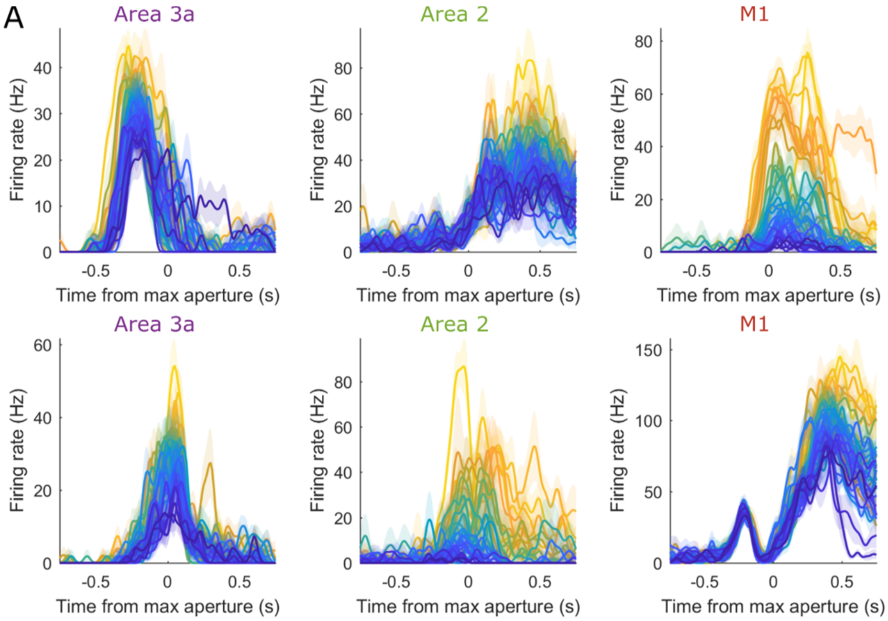

Figure S2. *Variety of neural responses.* Related to Figure 2. Example peri-event time histograms (PETHs) from 6 neurons across sensorimotor cortices that illustrate the variety of observed response profiles. PETHs are aligned to maximum aperture. Different colors indicate different objects, ranked from weakest to strongest response on a neuron-by-neuron basis; color maps are determined by rank order of maximum firing rate and thus differ across panels.

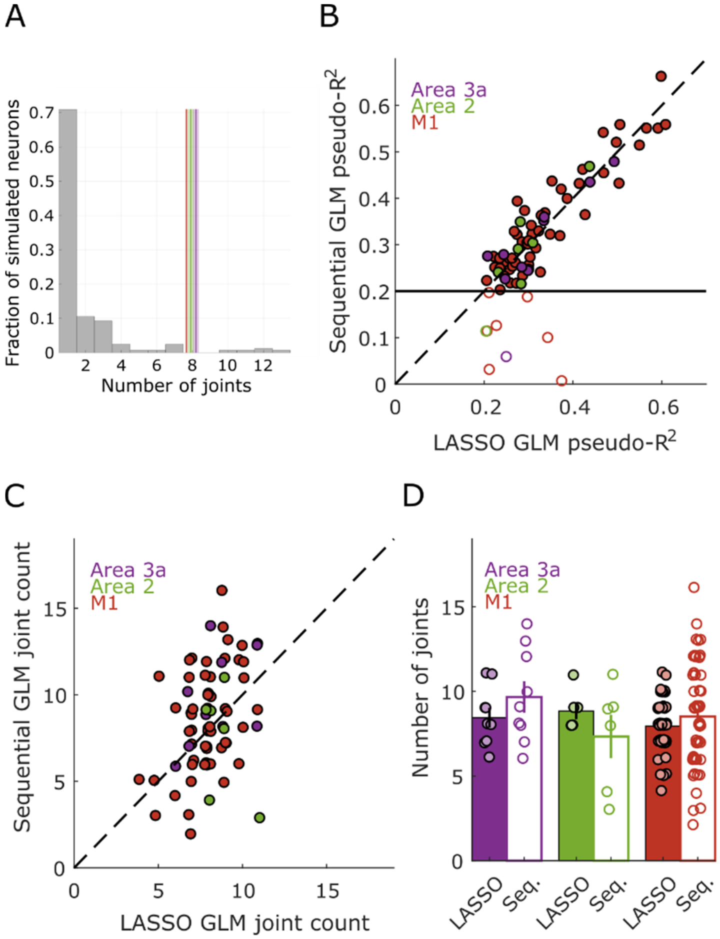

Figure S3. *Further testing of response field (RF) size results.* Related to Figure 4. **(A)** Distribution of inferred RF sizes for simulated neurons with single-joint RFs given recorded grasping behavior (see Methods). Each simulated neuron's RF size is inferred using the same GLM regression weight procedure illustrated in Figure 4B. Shown are the joint counts only for those simulated neurons with pseudo-R^2 > 0.05 (162/231). In the vast majority of cases, LASSO extracts a single-joint RF. Multi-joint RFs are therefore not an inevitable consequence of inter-joint correlations during grasp. Vertical lines indicate mean joint counts from each cortical area (bar heights from Figure 4C). Shaded regions around each line indicate ±1 standard error of the mean. **(B-D)** Testing RF size using a sequential, rather than LASSO, GLM procedure. **(B)** Sequential (ordinate) and LASSO (abscissa) GLMs yield similar goodness-of-fit in most cases (filled circles above the horizontal line). A repeated-measures ANOVA, with LASSO pseudo-R^2 and sequential pseudo-R^2 as the repeated measures and cortical area as a between-neuron factor, revealed no significant difference between the two measures ($F(1,68)=0.0398$, $p=0.8424$) nor did it reveal a significant difference across areas ($F(2,68)=0.0816$, $p=0.9217$). Only units with pseudo-R^2 > 0.2 for both LASSO and sequential GLM (thus excluding neurons denoted by the open circles in panel B) were selected for this analysis and those shown in panels (C) and (D) (10 units from area 3a, 7 from area 2, and 66 from M1). Diagonal dashed line indicates the unity line. **(C)** Scatter plot of the number of joints in each neuron's RF predicted with LASSO GLM as illustrated in Figure 4B (abscissa) against the RF size determined using the sequential GLM procedure (ordinate) (see Methods). There is considerable spread on a neuron-by-neuron basis, but both methods converged on similarly sized RFs. Diagonal dashed line indicates unity line. **(D)** Bar plots showing the mean results in (C) split by cortical field. Filled bars indicate the number of joints in the RF indicated by the LASSO model; open bars, by the sequential GLM model. Individual points indicate single neurons, with filled points being RFs assessed with LASSO, and open points being those assessed with sequential GLM. Error bars denote ±1 standard error of the mean. Repeated-measures ANOVA with LASSO RF size and sequential RF size as the repeated measures and cortical area as the between-subjects factor revealed no significant effect of the type of GLM employed ($F(1,68)=0.0374$, p=0.8473) nor did it reveal differences across areas ($F(2,68)=1.8544$, p=0.1644).

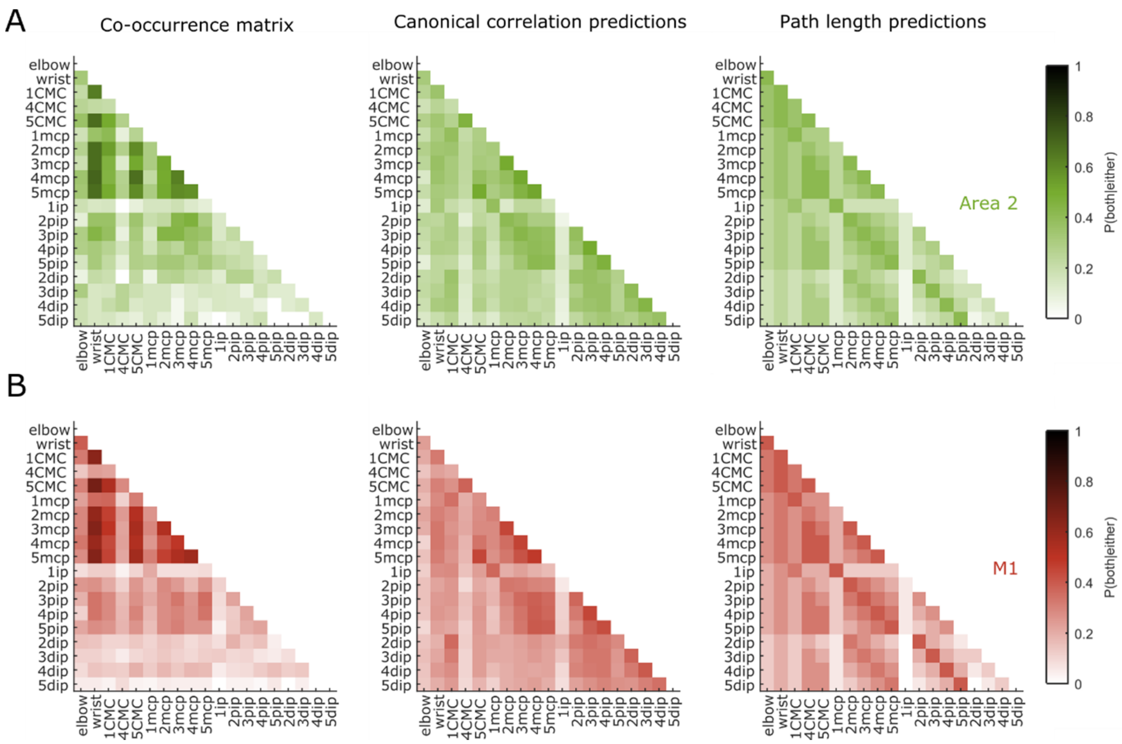

Figure S4. *Co-occurrence matrices for area 2 and M1*. Related to Figure 4. **(A-B)** Similar to Figure 4 panels D-F in the main text, but instead showing co-occurrence matrices across neurons in **(A)** area 2 and **(B)** M1. Just as in area 3a, inter-joint correlations and anatomical proximity do not account for the co-occurrence of pairs of joints in neurons' RFs (Correlation - Area 2: R^2 = 0.268; M1: R^2 = 0.253. Anatomical proximity (path length) - Area 2: R^2 = 0.253; M1: R^2 = 0.343). Axis tick labels follow the same conventions as Figure 4D-F.

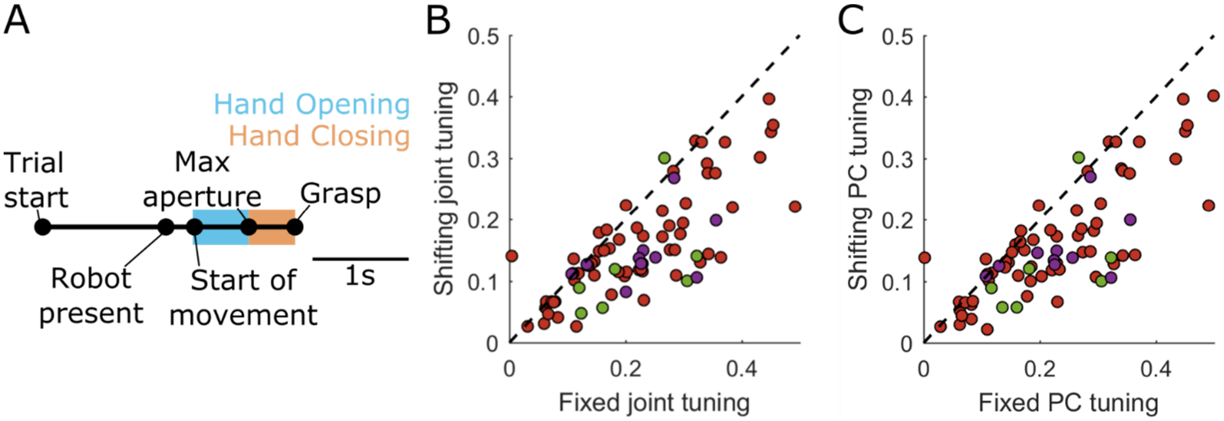

Figure S5. *Tests for shifts in neural tuning between different grasp epochs.* Related to Figure 5. **(A)** Task timeline as depicted in Figure 1, with the split epochs ("hand opening" and "hand closing") highlighted. We divided the task into two epochs to determine if differences in kinematics or neural tuning across these epochs may trivially give rise to large RFs when RFs are assumed to be consistent throughout grasp. **(B)** Cross-validated pseudo-R^2 of LASSO GLMs fit to joint angles and angular velocities over the entire movement epoch (abscissa) against those that permit the weight vector to change between hand opening and closing epochs (ordinate). Permitting the neural tuning to shift between epochs actually proves to be detrimental to model performance. **(C)** Same as (B), but for models fit to PC scores and their derivatives. Only units with pseudo-$R^2 > 0.2$ were included in this analysis (10 units from area 3a, 7 from area 2, and 66 from M1).

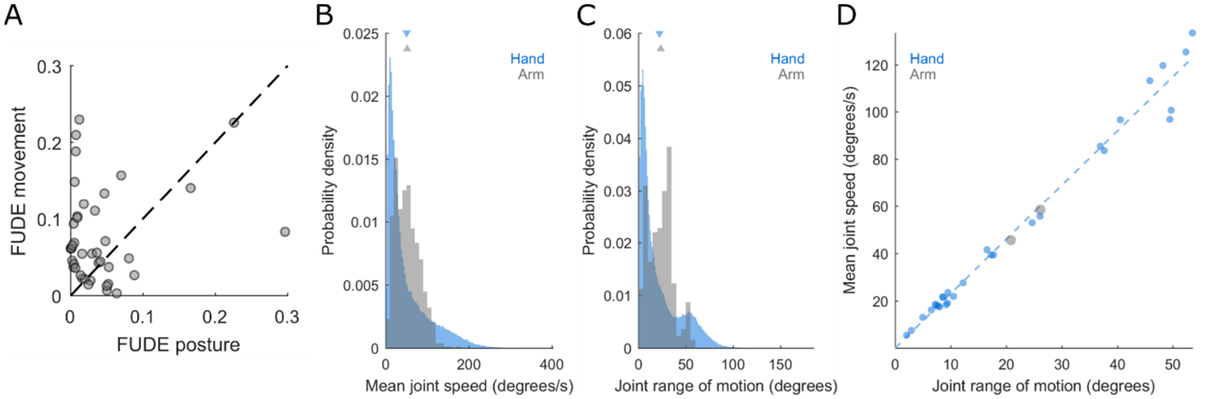

Figure S6. *Neural preference for velocity during reaching is not a trivial function of the statistics of task kinematics*. Related to Figure 6. **(A)** Similar to Figure 6B-D, only showing the fraction of unique deviance explained (*FUDE*) by posture and movement models for M1 neurons during reaching (Hatsopoulos, Xu, & Amit 2007). The majority of neurons fall above the diagonal. In other words, more unique deviance in M1 firing rates is explained by the time-varying movements of the proximal limb than by its posture, during reaching. This is consistent with previous reports (Paninski, Fellows, Hatsopoulos, & Donoghue 2004, Wang, Chan, Heldman, & Moran 2007) and shows that GLMs do not inherently perform better with postural predictors. **(B-D)** We further test whether the kinematic structure of reaching and grasping are different in a way that trivially explains neurons' different preferences during these tasks. **(B)** The probability density histograms of mean joint angular speed, where each instance is the mean speed of a single joint degree of freedom (DOF) during a single trial. For each histogram, instances are pooled from across joint DOFs, sessions, and animals. **(C)** The density histogram of per-trial range of motion, where each instance is the difference between the maximum and minimum angle of a joint DOF during a single trial. Instances are similarly pooled across joint DOFs, sessions, and animals. **(D)** The relationship between the average speed and average range of motion on a per-DOF basis. Neither the mean joint angular speed (two-sample equal-variance *t*-test, *t*(202780)=0.6541, *p*=0.5131) nor the joint angular range of motion (*t*(202780)=1.8462, *p*=0.0649) differs between reach and grasp. Moreover, the two DOFs tracked during reach follow the same trend as joint DOFs during grasp (R^2 = 0.9820). In other words, grasping and reaching movements are associated with overlapping distributions of joint angular speeds and ranges of motion. Neurons' preference for posture during grasp and movement during reach is therefore unlikely to be a consequence of the relative speeds or postural varieties of these tasks.

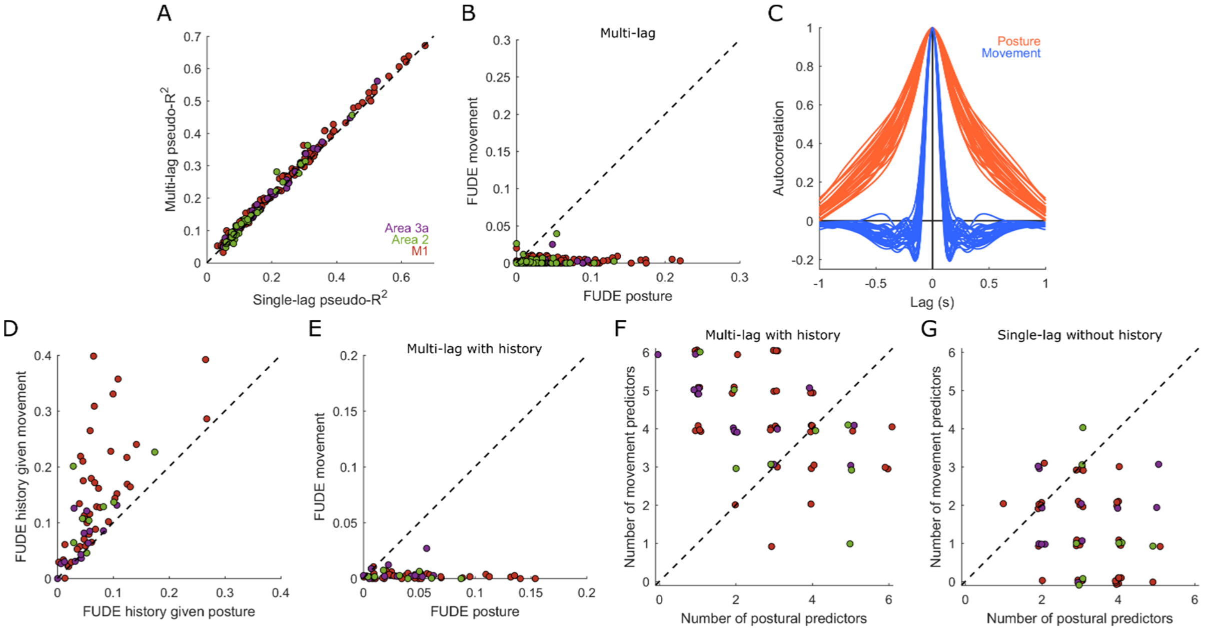

Figure S7. *Reconciling observed posture preference with past results that seem to show the opposite reveals posture preference to be the far more reliable outcome*. Related to Figure 6. **(A)** The previous report (Saleh et al. 2010) uses GLMs that fit kinematic trajectories comprising multiple latencies to the spiking activity of neurons. In the present study, we use kinematics at a single optimal latency for ease of interpretation. We observe a significant, but small, improvement in goodness-of-fit (pseudo-R^2) when using predictors at multiple latencies (paired-samples t-test, $t(234)=13.17$, $p=5.11\text{e-}30$, 95% confidence interval = [0.0089, 0.0121]). For these analyses, we only consider neurons with pseudo-$R^2 > 0.05$ for either the single- or multi-latency model (32 units from area 3a, 36 from area 2, and 167 from M1). **(B)** Even with multi-latency models, the fraction of unique deviance explained (*FUDE*) by postural predictors (abscissa) greatly exceeds that by movement predictors (ordinate). Here, only units with pseudo-$R^2 > 0.05$ for the multi-lag model are considered (30 from area 3a, 34 from area 2, and 161 from M1). **(C)** Mean autocorrelation functions of each of the 30 posture and movement degrees of freedom (DOFs). Each trace indicates the average of a DOF's autocorrelograms across all trials across all animals. The previous report uses GLMs that include spike history terms, which could preferentially affect deviance explained by the more strongly autocorrelated postural predictors. **(D)** The *FUDE* of spike history after accounting for hand posture predictors (abscissa) is indeed lower than that after accounting for hand movement predictors (ordinate), suggesting that the overlap between spike history and posture is greater than that between history and movement. For the analyses in this and all following panels, only a subset of units with pseudo-$R^2 > 0.2$, as assessed using either a single- or multi-latency model, was selected (13 units from area 3a, 8 from area 2, and 42 from M1). **(E)** Even when accounting for spike history, the *FUDE* of postural models (abscissa) far exceeds that of movement models (ordinate). **(F)** The previous report performed sequential GLM and counted the number of posture and movement predictors that emerged from these models. We use the 90%-of-squared-norm criterion (Figure 4B) to approximate this process (see Figure S3). GLMs that incorporate spike history terms and multi-latency predictors tend to comprise more movement (ordinate) than posture (abscissa) degrees of freedom. This replicates previous findings but contradicts *FUDE*, likely reflecting these GLMs' ability to fit multi-latency filters that approximate numeric integration. **(G)** When analyzing single-latency models without spike history terms, neurons' RFs tend to comprise fewer movement (ordinate) than posture (abscissa) predictors, consistent with the relative *FUDE* of the two. The number of predictors is smaller for panels D-G than in the main text because GLMs are fit to the reduced predictor set used in Saleh et al., 2010.